RETRIEVAL OF LATENT HEATING FROM TRMM MEASUREMENTS

BY W.-K. TAO, E. A. SMITH, R. F. ADLER, Z. S. HADDAD, A. Y. HOU, T. IGUCHI, R. KAKAR, T. N. KRISHNAMURTI, C. D. KUMMEROW, S. LANG, R. MENEGHINI, K. NAKAMURA, T. NAKAZAWA, K. OKAMOTO, W. S. OLSON, S. SATOH, S. SHIGE, J. SIMPSON, Y. TAKAYABU, G. J. TRIPOLI, AND S. YANG

TRMM-based latent heating products—not long ago considered out of our technological reach—are beginning to contribute to global modeling, but the necessary retrieval algorithms produce varying results and will require further research.

Precipitation, in driving the global hydrological cycle, strongly influences the behavior of the Earth's weather and climate systems and is central to their variability. Two-thirds of the global rainfall occurs over the Tropics,[1] which leads to its profound effect on the general circulation of the atmosphere. This is because its energetic equivalent, latent heating (LH), is the tropical convective heat engine's primary fuel source as originally emphasized by Riehl and Malkus (1958). At low latitudes, LH stemming from extended bands of rainfall modulates large-scale zonal and meridional circulations and their consequent mass overturnings (e.g., Hartmann et al. 1984; Hack and Schubert 1990). Also, LH is the principal energy source in the creation, growth, vertical structure, and propagation of long-lived tropical

[1] The Tropics are liberally taken as the area bounded by the 25°N–25°S latitude zone.

AFFILIATIONS: TAO, SMITH, ADLER, HOU, MENEGHINI, AND SIMPSON—Laboratory for Atmospheres, NASA Goddard Space Flight Center, Greenbelt, Maryland; HADDAD—NASA Jet Propulsion Laboratory–California Institute of Technology, Pasadena, California; IGUCHI AND SATOH—National Institute of Information and Communications Technology, Tokyo, Japan; KAKAR—NASA Headquarters, Washington, DC; KRISHNAMURTI—Department of Meteorology, The Florida State University, Tallahassee, Florida; KUMMEROW—Department of Atmospheric Science, Colorado State University, Fort Collins, Colorado; LANG—Science Systems and Applications, Inc., Greenbelt, Maryland; NAKAMURA—Hydrospheric Atmospheric Research Center, Nagoya University, Nagoya, Japan; NAKAZAWA—Japan Meteorological Agency, Meteorological Research Institute, Tsukuba, Japan; OKAMOTO AND SHIGE—Department of Aerospace Engineering, Osaka Prefecture University, Sakai, Osaka, Japan; OLSON—UMBC Joint Center for Earth Systems Technology, Baltimore, Maryland; TAKAYABU—Center for Climate System Research, University of Tokyo, Tokyo, Japan; TRIPOLI—Department of Atmospheric and Oceanic Sciences, University of Wisconsin—Madison, Madison, Wisconsin; YANG—School of Computational Sciences, George Mason University, Fairfax, Virginia
CORRESPONDING AUTHOR: Dr. Wei-Kuo Tao, NASA Goddard Space Flight Center, Code 613.1, Greenbelt, MD 20771
E-mail: tao@agnes.gsfc.nasa.gov

The abstract for this article can be found in this issue, following the table of contents.

DOI:10.1175/BAMS-87-11-1555

In final form 26 May 2006

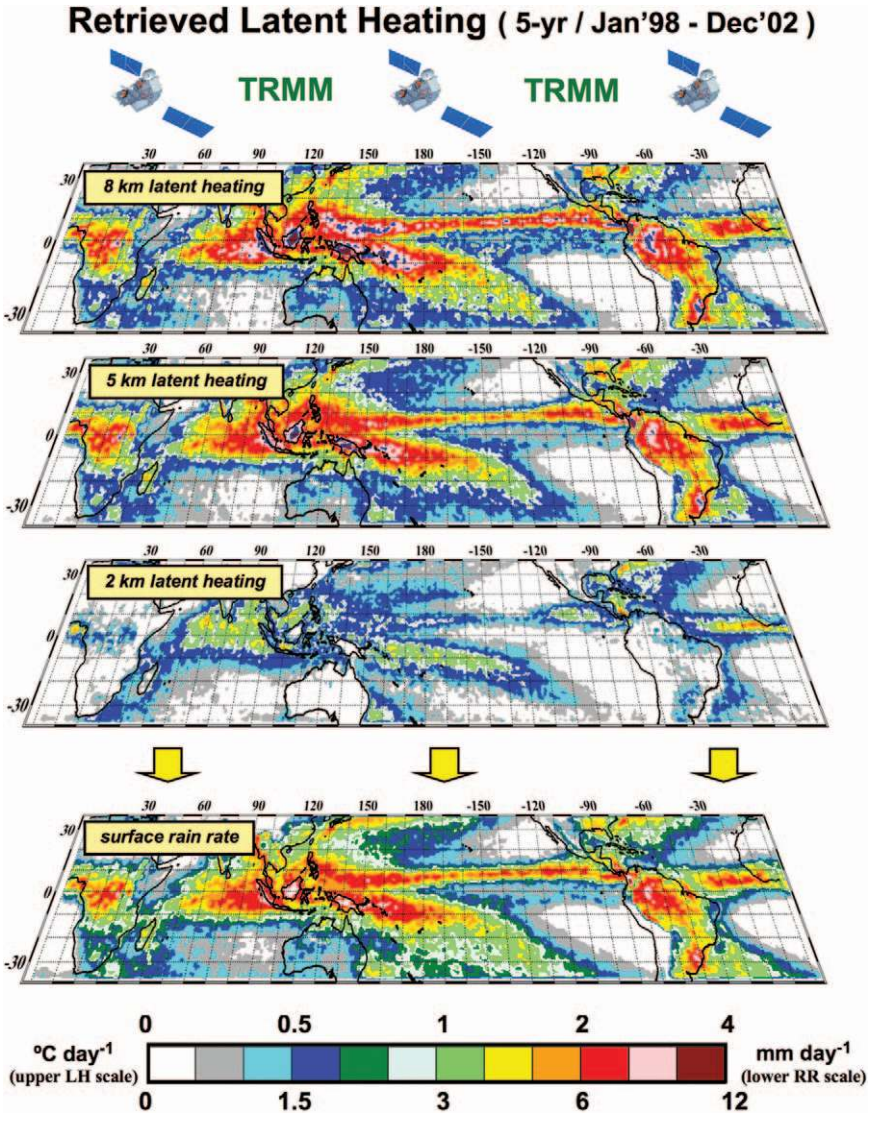

Fig. 1. (upper three panels) Five-year mean Q_1 heating rates at 8, 5, and 2 km AGL (upper 3 panels) along with (bottom) surface rain rates over global Tropics determined by GSFC CSH algorithm applied to 1998–2002 PR measurements acquired from the TRMM satellite.

waves (e.g., Puri 1987; Lau and Chan 1988). Moreover, the distinct vertical distribution properties of convective and stratiform LH profiles help influence climatic outcomes via their tight control on large-scale circulations (Lau and Peng 1987; Nakazawa 1988; Sui and Lau 1988; Emanuel et al. 1994; Yanai et al. 2000; Sumi and Nakazawa 2002; Schumacher et al. 2004).

The purpose of this paper is to describe how LH profiles are being derived from satellite precipitation rate retrievals, focusing on those being made with Tropical Rainfall Measuring Mission (TRMM) satellite measurements. As an example, Fig. 1 provides an illustration of averaged patterns of LH determined from five years of TRMM measurements (1998–2002), mapped at three vertical levels (2, 5, and 8 km), along with the associated averaged surface rain-rate map (this diagram is discussed in detail in "Temporal and spatial averages").

The TRMM satellite is the centerpiece of a joint rainfall mission between the American and Japanese space agencies, the National Aeronautics and Space Administration (NASA) and the Japan Aerospace Exploration Agency [(JAXA); formerly the National Space Development Agency of Japan (NASDA)], providing the first high-quality rainfall and space–time structures of LH over the global Tropics and subtropics (see Simpson et al. 1996). The TRMM observatory was launched in November 1997, in a 350-km orbit inclined 35° to the Earth's equatorial plane (in August 2001, the orbit was boosted to ~400 km to preserve fuel by reducing atmospheric drag). The main rain instruments are JAXA's Ku-band Precipitation Radar (PR) and NASA's nine-channel TRMM Microwave Imager (TMI).

Studies of latent heat estimation from satellites date back to the first spaceborne passive microwave (PMW) rain radiometer [see, e.g., a study by Adler and Rodgers (1977) concerning total column LH within tropical cyclones]. Latent heating is that portion of diabatic heating that is either released or absorbed within the atmosphere as a result of the phase changes of water (i.e., from gas to liquid, liquid to solid, gas to solid, and their reverse processes). The related terms are condensation–evaporation, freezing–melting, and deposition–sublimation. Latent heating is dominated by phase changes between water vapor and small liquid or frozen cloud-sized particles. These processes are not directly detectable with current remote

sensing or in situ instruments, which explains why the retrieval schemes to be discussed depend heavily on some type of cloud-resolving model (CRM).

CRMs require detailed physical parameterizations, particularly for a) radiative transfer, b) surface radiation, heat, moisture, and momentum fluxes, c) boundary layer heat, moisture, and momentum turbulent transport, and d) cloud microphysics. These specialized physics are needed for simulating dynamical interactions of individual clouds and cloud ensembles within the large-scale environment. The studies of Soong and Tao (1980, 1984) were some of the first to use CRMs for understanding interactions between clouds and their environment. Early CRMs credibly reproduced the statistical properties of clouds as noted by Lipps and Hemler (1986), Tao and Soong (1986), and Tao et al. (1987), and later were corroborated by Krueger (1988) in a detailed study and by others in specialized applications (e.g., Tripoli and Cotton 1989a,b). Since the TRMM launch, and in anticipation of the future Global Precipitation Measurement (GPM) Mission (Smith et al. 2006), modern CRMs are used to simulate phase changes of water and mass transfers of water species in support of LH retrieval, notably the Goddard Cumulus Ensemble (GCE) model (Tao and Soong 1986; Tao and Simpson 1993; Tao 2003; Tao et al. 2003), the University of Wisconsin (UW) Nonhydrostatic Modeling System (NMS; Tripoli 1992a,b, Tripoli and Smith 2006, manuscript submitted to *Mon. Wea. Rev.*), and the fifth-generation Pennsylvania State University (PSU)–National Center for Atmospheric Research (NCAR) Mesoscale Model (MM5) (Dudhia 1993).

Under the Boussinesq approximation, the thermodynamic (or temperature) budget can be explicitly calculated from CRMs as

$$Q_1 - Q_R = \overline{\pi}[-(1/\overline{\rho})(\overline{\partial\overline{\rho}w'\theta'/\partial z}) - \overline{\nabla \bullet V'\theta'}] + (1/c_p)[L_v(c-e) + L_f(f-m) + L_s(d-s)], \quad (1)$$

where the primes indicate deviations from the large-scale environment mainly due to small-scale cloud processes. The variable θ is potential temperature, $\overline{\rho}$ is air density, $\overline{\pi} = (p/P_{00})^{R/c_p}$ is nondimensional pressure (where p and p_{00} are dimensional and reference pressures with p_{00} taken as 1000 hPa), and c_p and R represent the specific heat at constant pressure and gas constant of dry air, respectively. The variables L_v, L_f, and L_s are the latent heats of condensation, freezing, and sublimation, respectively, while the variables (*c, e, f, m, d, s*) denote rates for 1) the condensation of cloud droplets, 2) evaporation of cloud droplets and rain drops, 3) freezing of water droplets and raindrops, 4) melting of ice crystals, snowflakes, graupel, and hail, 5) deposition of ice crystals, and 6) sublimation of all ice hydrometeors, respectively.

The term $(1/c_p)$ $[L_v(e-e) + L_f(f-m) + L_s(d-s)]$ is the LH due to microphysical phase changes. As defined in Yanai et al. (1973), Q_1 is the apparent heat source, while Q_R is the radiative heating rate associated with radiative transfer processes. The first two terms on the right-hand side of Eq. (1) are the vertical and horizontal eddy heat flux convergence

$$[\overline{\pi}(\overline{\partial w'\theta'/\partial z}), \text{ and } \overline{\pi}(\overline{\nabla \bullet V'\theta'})],$$

where the horizontal diffusion term is neglected when Eq. (1) is spatially averaged over a large area suitable for large-scale diagnostic analysis.

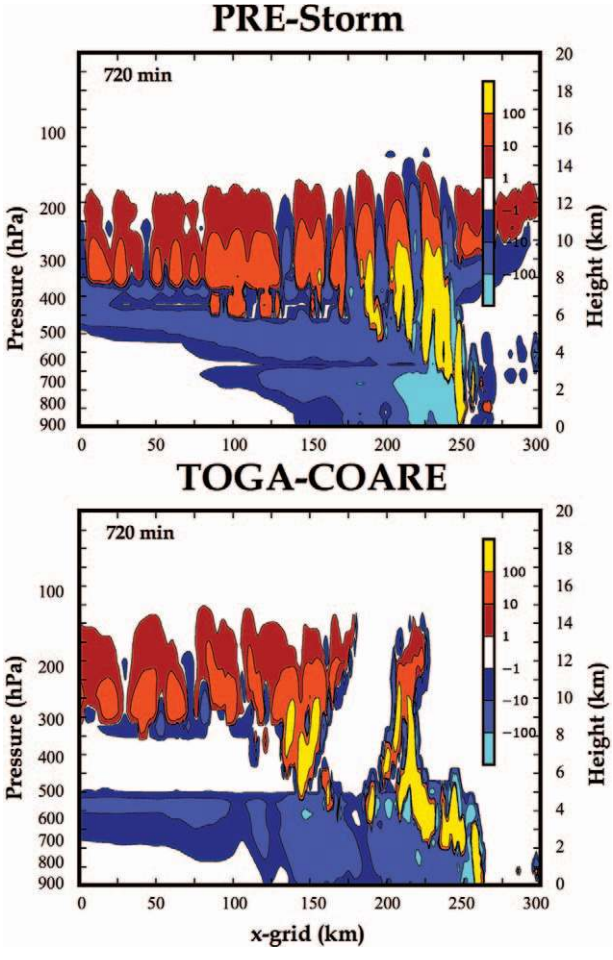

Fig. 2. Height–length cross sections of GCE CRM-generated LH (°C day^{-1}) consisting of sum of heating by condensation, freezing, and deposition, and cooling by evaporation, melting, and sublimation, associated with (top) midlatitude continental (PRE-STORM) squall line and (bottom) tropical oceanic (TOGA COARE) MCS. [Simulations are discussed in Tao et al. (1993a, 1995, 1996), Wang et al. (1996), and Lang et al. (2003).]

Figure 2 illustrates the instantaneous LH structures associated with both a midlatitude and a tropical mesoscale convective system (MCS) simulated by the GCE CRM in a two-dimensional framework. The cases were drawn from two field campaigns, the midlatitude continental Preliminary Regional Experiment for Storm-Scale Operational and Research Meteorology (PRE-STORM) and tropical oceanic Tropical Ocean Global Atmosphere Coupled Ocean–Atmosphere Response Experiment (TOGA COARE).[2] Evident in the figure are 1) condensation heating in the lower to middle troposphere of the convective leading edge of the cloud systems, 2) deposition heating in the upper parts of the convective and stratiform regions, 3) cooling at low levels in the stratiform regions stemming from evaporation of rain, 4) cooling from melting of precipitation particles in a narrow layer near the freezing level, and 5) cooling from sublimation adjacent to depositional heating in the stratiform regions.

The alternating heating–cooling pattern at upper levels is caused by gravity wave dispersion induced by deep convection. This is more significant for the midlatitude case because the associated convective updrafts are stronger. Also, cooling within the stratiform region is larger and deeper for midlatitudes due to the generally drier environments. Finally, the level separating the heating and cooling layers within the stratiform regions (i.e., the melting level) is different for the two systems. The simulated squall line structures are generally consistent with observed squall lines (e.g., Biggerstaff and Houze 1991; and Jorgensen et al. 1997).

Using a residual approach, Q_1 can be derived indirectly over a spatial domain by measuring profiles of temperature, pressure, and the three-dimensional wind vector from a suitably spaced circumscribing network of radiosondes. This "diagnostic heat budget" methodology was first described by Yanai et al. (1973) and has been extensively studied by others (e.g., Nitta 1977; Houze 1982, 1989, 1997; Johnson 1984). It can be expressed by

$$Q_1 = \overline{\pi}\left(\frac{\partial \overline{\theta}}{\partial t} + \overline{V} \bullet \nabla \overline{\theta} + \overline{w}\frac{\partial \overline{\theta}}{\partial z}\right). \qquad (2)$$

There is an accompanying equation for the apparent moisture sink or drying (Q_2) similar to Eq. (2), except that $\overline{\theta}$ and Q_1 are replaced by water vapor specific humidity ($\overline{q}$) and negative Q_2, respectively.

Latent heating estimates from satellite precipitation rate profiles can be assessed from Q_1 budgets determined in CRM simulations, from regional- and large-scale prediction models, and from global climate reanalysis products (Nigam et al. 2000). Because current LH retrieval schemes are all tied to CRMs, a more independent approach for validating TRMM LH estimates is to use the radiosonde-based diagnostic heat budget approach discussed above. For purposes of this study, Q_1 budgets diagnosed from sounding observations taken during three TRMM field campaigns [South China Sea Monsoon Experiment (SCSMEX), TRMM Large Scale Biosphere–Atmosphere Experiment in Amazonia (LBA), and the Kwajalein Experiment (KWAJEX)] and other past and current field campaigns [Global Atmospheric Research Programme (GARP) Atlantic Tropical Experiment (GATE), PRE-STORM, TOGA COARE, and the Department of Energy's (DOE's) Atmospheric Radiation Measurement (ARM) Program][3] are used as the principal validation datasets.

In "Descriptions of latent heating algorithms," a set of five LH algorithms developed for TRMM applications are described; "Heating structures estimated from individual algorithms" presents highlights from various applications of the algorithms; "Global modeling applications" describes how LH products are currently being used in conjunction with global weather and climate models; and finally "Final remarks and recommended future research" offers discussion and remarks intended to stimulate further research.

DESCRIPTIONS OF LATENT HEATING ALGORITHMS. In this section, brief descriptions are provided for five different LH algorithms designed

[2] PRE-STORM Central took place in Kansas and Oklahoma during May–June 1985 (Cunning 1986). TOGA COARE took place over the Pacific Ocean warm pool from November 1992 to February 1993 (Webster and Lukas 1992; Nakazawa 1995).

[3] SCSMEX took place over the South China Sea during May–June 1998 (Lau et al. 2000); LBA took place in Rondonia, Brazil, during January–February 1999 (Halverson et al. 2002; Petersen et al. 2002); KWAJEX took place in the vicinity of Kwajalein Atoll, Marshall Islands, during July–September 1999 (Yuter et al. 2005); GATE took place over the eastern tropical Atlantic Ocean during June–September 1974 (GATE International Scientific and Management Group 1974; Houze and Betts 1981); and the DOE ARM Program supports experiments in Oklahoma at DOE ARM's Southern Great Plains (SGP) Cloud and Radiation Test Bed (CART) site (Stokes and Schwartz 1994).

for applications with satellite-generated precipitation rate profile inputs, with attention given to TRMM products. They are referred to as the 1) Goddard Convective–Stratiform Heating (CSH) algorithm, 2) Goddard Profiling Heating (GPROF Heating) algorithm, 3) Hydrometeor Heating (HH) algorithm,

Table 1. Summary of CSH, GPROF Heating, HH, PRH, and SLH algorithms, in which key references, essential algorithm input parameters, past case studies, and relevant space–time resolutions of heating calculations are provided. Wherever + symbols precede citations in the "References" column, corresponding + symbols in other columns denote associated information vis à vis those citations. In the "Alg" column, "RECON" indicates reconstruction algorithm (i.e., heating is calculated by using model-generated parameters of surface rain rate and convective/stratiform fractions as input to the CSH heating algorithm), "COMB" indicates combined PR–TMI algorithm, and SSM/I indicates Special Sensor Microwave Imager, which is a PMW radiometer used on Defense Military Satellite Program (DMSP) satellites. In the "Resolution" column, inst indicates instantaneous, hr indicates 1 hr, dy indicates 1 day, and mo indicates 1 month.

Alg	References	Input parameters	Cases	Resolution
CSH (RECON: SSM/I	Tao et al. (1993b)	• Surface rain rate and convective/stratiform fractions	• GATE (1974) • PRE-STORM (1985) • Tropical Cyclone Thelma 1987	200–300 km; dy
CSH (RECON: PR)	+ Tao et al. (2000) + Tao et al. (2001) + This study	+ Surface rain rate and convective/stratiform fractions + CSH, GPROF Heating, and HH algorithm outputs + Surface rain rate and convective stratiform fractions	+ TOGA COARE (1992–93) + Various tropical regimes (February 1998) + Global Tropics (December 1997–November 2000)	+ 500 km; 3–6 hr + 110 km; dy + 55 km; mo
GPROF (SSM/I; TMI)	+ Olson et al. (1999) + Olson et al. (2006) + Yang et al. (2006) + This study	• Lookup table linking CRM-generated hydrometeor density/$Q_I - Q_R$ profiles and radiative transfer equation (RTE) model-generated PMW TBs	+ Hurricane Andrew (1992) + Tropical MCSs (1992) + TOGA COARE (1992–93) + Squall line	+ 25 km; inst + 25 km; inst + 500 km; dy + 28 km; inst
HH (RECON)	Tao et al. (1990, 1993b) Simpson and Tao (1993)	• Surface rain rate for all precipitation categories • Hydrometeor density profiles (cloud/rain/ice crystal/snow/aggregate/graupel) • PRE-STORM (1985) • Terminal velocities of rain/snow/aggregate/graupel hydrometeors	• GATE (1974) • EMEX (1987)	+ 15 km; inst + 15 km; inst + 15–50 km; inst + 275 km; mo + 5 km; inst
HH (SSM/I; PR; TMI; COMB)	+ Smith et al. (1992, 1994a) + Smith et al. (1994a, 1994b) + Yang and Smith (1999a, 2000) + Yang and Smith (1996b) + This study	• Frozen and/or liquid rain-rate profile (s)	+ Tropical Cyclones Thermal 1987/Hugo 1989 + TOGA COARE (1992–93) + TOGA COARE (1992–93) + Global Tropics (1992) + Hurricane Bonnie 1998	5–100 km; inst
PRH (PR)	Satoh and Noda (2001) This study	• Surface rain rates for all precipitation categories • Terminal velocities of rain hydrometeors • Cloud vertical velocities • Precipitation top height (PTH) • Bright band and cloud-base heights	• Squall line in Oklahoma	*5–100* km; inst
SLH (RECON)	Takayabu (2002) Shige et al. (2004) This study	• Surface rain rates for all precipitation categories • Convective/stratiform/anvil classification • PTH • Rain rate at and height of melting level	• TOGA COARE (1992–93)	*5–100* km; inst

4) Precipitation Radar Heating (PRH) algorithm, and 5) Spectral Latent Heating (SLH) algorithm. The CSH, GPROF, and SLH algorithms require the full complement of cloud model data generated by a CRM. Table 1 summarizes algorithm features, including principal authorship, key algorithm inputs, identification of satellite datasets to which the algorithms have been applied, and the notational space–time resolutions associated with the algorithms. As an aid to understanding these algorithms and interpreting their results, a compilation of their "general" strengths and weaknesses is provided in Table 2, while full explanations are provided in Tao et al. (2006, manuscript submitted to *Mon. Wea. Rev.*).

A preliminary comparison between earlier versions of three of the algorithms (CSH, GPROF Heating, and HH) was performed with February 1998 TRMM data by Tao et al. (2001). An important finding was the overall equivalence in the horizontal distributions of latent heat release produced by the three schemes and the close relationships of these distributions to surface rainfall. They all were able to identify areas of major convective activity, including well-defined sectors of the intertropical convergence zone (ITCZ) within

Table 2. General strengths and weaknesses of CSH, GPROF Heating, HH, PRH, and SLHI algorithms.

Algorithm	General strengths	General weaknesses
CSH	• CRM-based and robust algorithm with long history. • Adaptable to any TRMM level-2 algorithm (PR, TMI, COMB). • Adheres to convective/stratiform heating variational characteristics based on diagnostic budget studies. • Extensive simulation and Q_1 validation studies involving field campaign datasets from GATE, EMEX, PRE-STORM, TOGA COARE, SCSMEX, TRMM LBA, KWAJEX, and DOE ARM programs.	• Restricted to convective/stratiform categories and sensitive to errors in corresponding cover fractions. • Imperfections and incompleteness in CRM-generated heating profiles defined in lookup table lead to systematic errors in retrieved profiles. • Zero surface rainfall leads to zero heating profiles aloft.
GPROF Heating	• CRM based in which diagnosed $Q_1 - Q_R$ profiles consistent with associated retrieved hydrometeor density profiles. • Random errors in retrieved $Q_1 - Q_R$ profiles well defined because of Bayesian framework. • $Q_1 - Q_R$ profiles retrievable instantaneously at TMI beam scale (~14 km) or at space–time-averaged scales.	• Hydrometeor density and $Q_1 - Q_R$ profiles have different temporal scales. • Errors in CRM/RTE model database simulations lead to systematic errors in retrieved $Q_1 - Q_R$ profiles. • Underrepresentation of CRM/RTE model-simulated hydrometeor density profiles linked to $Q_1 - Q_R$ profiles in database leads to $Q_1 - Q_R$ representativeness errors.
HH	• Physically based and direct microphysics approach with long history. • Adaptable to any TRMM level-2 precipitation profile algorithm (PR, TMI, COMB). • LH profile vertical structure closely related to vertical rain-rate gradients, accurate precipitation mass flux inputs result in small systematic errors. • LH profiles retrievable instantaneously at either PR or TMI beam scales (~5 or ~14 km, respectively) or at space–time-averaged scales.	• Sensitive to noise in retrieved precipitation profiles, i.e., noise in hydrometeor density or rain-rate profiles passed on to LH profiles. • Greater uncertainties generated from errors in formulation of hydrometeor terminal velocities, more so at upper levels. • Lesser uncertainties generated without knowledge of cloud-scale vertical motion, must be assumed zero if unknown.
PRH	• Produces distinct LH profiles for various types of organized precipitation systems (e.g., squall lines, tropical cyclones, MCSs). • Differentiated cloud vertical velocities provided for convective, stratiform, and deep anvil precipitation categories. • LH profiles retrievable at instantaneous scale from PR.	• Sensitive to estimated vertical velocities and hydrometeor density (or rain rate) profiles, especially for mixed phase. • Uses idealized thermodynamic assumptions, and may produce cooling near cloud top and in upper part of cloud. • Limited sampling due to PR's narrow swath width.
SLH	• Differentiates heating structures between shallow convective and deep • Produces heating profiles for decaying anvil stage even with zero surface rain rate. • Heating profiles retrievable at instantaneous scale from PR.	• Restricted to convective/shallow stratiform/anvil stratus categories and sensitive to errors in corresponding cover fractions. • Imperfections and incompleteness in CRM-generated heating profiles defined in lookup table lead to systematic errors in retrieved heating profiles. • Limited sampling due to PR's narrow swath width.

the central and east Pacific, and along the southern Pacific convergence zone (SPCZ). The only significant differences between the algorithms pertained to the derived altitudes of maximum heating. In all cases, the CSH estimates exhibited one heating level maximum with the level varying between different geographic locations—features in general agreement with diagnostic budget studies.

A broader heating maximum, often with two embedded peaks, was obtained with the GPROF and HH algorithms. This type of vertical heating structure resulted from these two algorithms averaging sets of individual LH profile solutions drawn from mixes of retrieved convective and stratiform precipitation rate profiles. In essence, the distinct LH structures, associated with the two underlying precipitation modes and controlled by fundamental differences in the two mode's characteristic precipitating ice profiles, combine under an averaging operator to produce a sharp and distinct minimum and an additional secondary maximum in the lower atmospheric layers.

While such structures are not normally found in diagnostic calculations, they are a realistic interpretation by the GPROF and HH algorithms of what are potentially flawed precipitating ice profiles produced by the precipitation rate retrieval algorithms preceding the application of the LH algorithms. Because all five of the algorithms are still undergoing development and improvement, and because comprehensive comparisons of the current versions of the algorithms with independent diagnostic estimates have yet to be performed, the general strengths and weaknesses can only be assessed in relative terms.

In such circumstances, the effects of differing physical assumptions on the various algorithms' diagnosed LH properties deserve careful attention. It is emphasized that the HH and PRH algorithms are similarly constrained by hydrometeor conservation under a steady-state assumption, but with different formulations for LH generation. The other three algorithms are directly CRM based, differing insofar as the cloud-type classification scheme, the lookup table indexing strategy, and the details of the precalculated lookup table heating profile entries. The CSH, SLH, and GPROF algorithms are designed to retrieve both LH and $Q_1 - Q_R$ because these schemes use cloud information directly generated by the CRM simulations, which exactly correspond to terms included in Eq. (1). In essence, the CRMs provide cloud database lookup tables consisting of both LH and $Q_1 - Q_R$. Alternatively, the HH and PRH algorithms are designed to estimate just the LH term because these schemes are tied directly to the vertically distributed structure of precipitation rate profiles, which may or may not have been generated by a precipitation rate algorithm utilizing a CRM for guidance.

HEATING STRUCTURES ESTIMATED FROM INDIVIDUAL ALGORITHMS. Application of the TRMM LH algorithms is being conducted over a range of space and time scales, from an order of 10 to 500 km spatially, and from instantaneous to monthly temporally. Although there is no preferred scale for calculating LH, there are a variety of current applications using LH products, with further research underway, to determine the optimal scales at which LH retrievals can be considered reliable.[4]

Instantaneous latent heating structure. Several of the TRMM LH algorithms determine instantaneous precipitation rates and heating profiles at satellite footprint resolution. The rationale for operating the algorithms at the highest possible resolution is that systematic errors in averages of high-resolution estimates of heating are generally less than the systematic error of a single heating estimate made at the scale of the average (i.e., the LH derivations represent nonlinear transforms of pixel-level precipitation rates). Therefore, even though instantaneous footprint-scale estimates may contain undesirable errors, spatial averaging and/or filtering can reduce random effects to acceptable levels, while ensuring that smoothed products contain a minimum of systematic error.

Figure 3 illustrates instantaneous, high-resolution (~4 km) rain rates and LH structures in an intense Atlantic tropical cyclone (Hurricane Bonnie) retrieved by the HH algorithm, based on the vertical derivative of rain mass flux from the combined PR–TMI algorithm. The structure of the hurricane eye and the convective rain spiral bands are properly captured. Precipitation mass appears at high altitudes in the presence of deep convection, such as around 200 km along the satellite's nadir track (seen in the middle panel). Widespread weaker rain rates are found between convective cells. In the weak rain areas, rain rates are mostly concentrated in the

[4] A comprehensive intercomparison and validation project involving five heating algorithms is now underway. It is examining multiple cases from full resolution to large scale, including validation with diagnostic calculations obtained from three NASA field experiment datasets, SCSMEX, TRMM LBA, and KWAJEX, plus two datasets from DOE's ARM CART program.

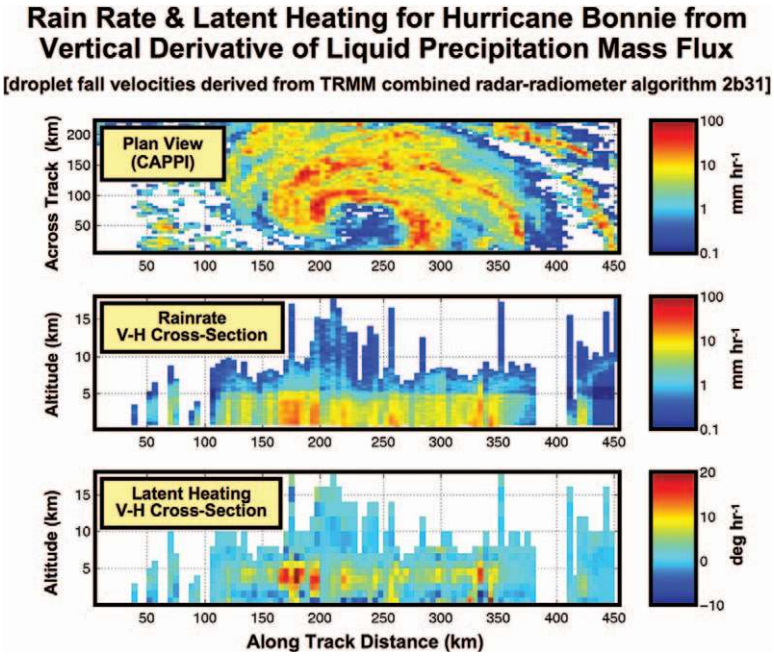

FIG. 3. (top) Plan view of near-surface rain rates for Hurricane Bonnie (22 Aug 1998) retrieved from combined algorithm [i.e., TRMM PR–TMI rain-rate algorithm described by Haddad et al. (1997) and Smith et al. (1997)]; (middle) vertical cross section of rain-rate profiles along satellite nadir track; (bottom) vertical cross section of LH profiles from HH algorithm along satellite nadir track. In all three panels, distances across (top) or along satellite nadir track are given in km.

middle to lower troposphere where stratiform conditions are prevalent. Deep LH is associated with the strongest convective cells (lower panel of figure). Peaks of maximum LH vary with different conditions. For example, one peak is located at 3–5 km at 180 km along nadir track, while another is at 3–4 km at 200 km along satellite track. Altitudes of the LH maxima are generally at or below 5 km. Evaporative cooling occurs in the lower troposphere in the stratiform regions.

Overall, the general structure of LH based on the HH algorithm is heuristically correct for a hurricane, although the level of maximum heating is lower than that found from other studies of tropical cyclones. This is because the current version of the combined PR–TMI algorithm (as well as the PR algorithm) does not produce precipitation by any but the largest frozen hydrometeors. By including the effect of all precipitating ice hydrometeors, the level of maximum heating would be elevated. (An experimental version of the combined algorithm now includes a frozen precipitation mode to account for all deposition–sublimation and freezing–melting processes above and below the melting level, enabling HH- and PRH-type algorithms to produce complete LH profiles with PR-based precipitation information.)

Figure 4 presents results from the GPROF Heating algorithm for a squall line in the tropical North Atlantic Ocean. The different panels include estimates of instantaneous surface rain rate, convective rain rate (rain mass assigned to convective category), and vertical cross sections spatially averaged to 28 km of the total precipitation mass content, along with $Q_I - Q_R$. The heaviest rains are seen along the convective leading edge of the system, while generally lower precipitation rate intensities are observed in the trailing stratiform areas to the north and west of the leading edge. The transect A–B is nearly perpendicular to the leading edge, traversing both the convective and stratiform regions. The leading-edge convection is characterized by relatively high precipitation mass contents, exceeding 1 g m^{-3} near the surface. Horizontally collocated with the maximum precipitation mass contents are maximum estimated heating rates, exceeding 9°C h^{-1} between 5- and 8-km altitude. Stratiform rains (horizontal coordinates less than 120 km) are associated with maximum precipitation mass contents at midlevels. The decrease of precipitation mass contents in the lower troposphere is due to the evaporation of rain, where cooling rates of ~ –1°C h^{-1} are estimated. The overall heating structures are similar to those in Fig. 2, except that the fine features simulated by the GCE CRM are not diagnosed due to the coarser resolution of the GPROF Heating algorithm's TMI radiance input.

Figure 5a shows instantaneous LH profiles retrieved by both the PRH and SLH algorithms, spatially averaged to 50-km resolution, associated with 1) a Pacific tropical cyclone (Typhoon Jelawat) in its developing stage (upper diagram), and 2) a MCS over the tropical ocean northwest of Australia (lower diagram). The PR-estimated rain rates used as input for these two algorithms are also shown. Overall, for the tropical cyclone case, there are several similarities between the PRH and SLH algorithm profiles. For example, both indicate strong heating on both sides of the eye. In addition, both algorithms exhibit strong

heating in a narrow shaft in the lower troposphere to the right of the eye. Away from the eyewall region, the heating patterns are similar to those observed and simulated by CRMs in the stratiform regions of MCSs (e.g., Houze 1982, 1997; Tao et al. 1993b, 2000; and Lang et al. 2003).

As expected, there are noteworthy differences between the two sets of heating profiles. First, PRH heating is confined to the same altitude range as that of the rainfall profiles, while SLH retrieves heating well above the rain. This is evident in larger heating amplitudes at higher altitudes in the horizontal mean profiles in Fig. 5a (two right-hand panels of upper diagram). Second, the SLH level of maximum heating is lower than that of PRH. Third, the cooling region retrieved using PRH in the lower troposphere is stronger than that from SLH. Fourth, PRH also produces low-level cooling in its convective region. Fifth, the SLH heating structure has smoother features because it uses a lookup table based on averaged CRM-generated profiles. On a final note, the general structure of the SLH-generated $Q_1 - Q_R$ and LH profiles are similar, except that the $Q_1 - Q_R$ profile has a larger maximum at a higher altitude (upper-right-hand panel of upper diagram).

The SLH and PRH LH analyses associated with an offshore Australian MCS are illustrated in the lower diagram of Fig. 5a. Again, the PR-estimated rain rates that are used as algorithm input are shown in the diagram. Strong heating (> 10°C h^{-1}) is associated with large rain rates (> 50 mm h^{-1}) in the convective region of the squall system. There is weak heating aloft and cooling below in the trailing stratiform region. Both averaged $Q_1 - Q_R$ and LH profiles peak at middle levels (about 6 km, according to the upper-right-hand panel of the lower diagram). For this case, the SLH-retrieved level of maximum heating is higher than that of the tropical cyclone case. This is because the convective system is in its mature stage while the tropical cyclone system is in its developing stage. That explains why the magnitudes of stratiform heating and cooling for the MCS case exceed those of the tropical cyclone. As is evident in the upper-right-hand panel, both the averaged $Q_1 - Q_R$ and LH profiles peak at middle levels (~6 km). This agrees well with the midtropospheric heating maximum found for the Australian Monsoon Experiment (AMEX) convective systems (Frank and McBride 1989). The estimated LH profile has a distinct cooling feature (relative minimum of heating) near 4 km due to melting processes. Conversely, the $Q_1 - Q_R$ profile does not indicate cooling near 4 km because the eddy heat flux convergence compensates for the cooling due to melting. As in the tropical cyclone case, PRH yields stronger cooling in the lower troposphere while SLH heating features are smoother.

Figure 5b shows the LH structure of a midlatitude squall line retrieved using only the PRH algorithm. The PR-observed radar reflectivities and estimated rain rates used as algorithm inputs are also shown. The radar reflectivity pattern is similar to that of an observed PRE-STORM squall line (Rutledge et al. 1988). Strong heating (> 10°C h^{-1}) is associated with large rain rates (> 50 mm h^{-1}) at the leading edge of the squall system. There is weak heating aloft and cooling below in the trailing stratiform region. These features are similar to those simulated by CRMs [e.g., Fig. 1b from Lang et al. (2003)], those observed (e.g.,

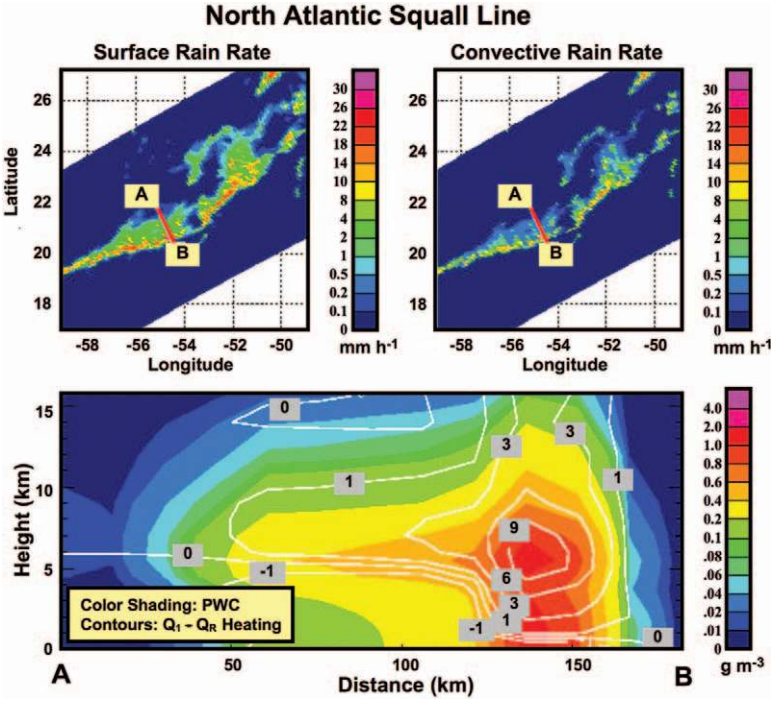

FIG. 4. (top left) Surface and (top right) convective rain rates for squall line in North Atlantic Ocean (7 Apr 1998) retrieved from GPROF algorithm [i.e., TMI rain-rate algorithm described by Kummerow et al. (1996, 2001) and Olson et al. (1999, 2006)]. (bottom) Height–length cross section (~28 km horizontal resolution) of total precipitation water content (color shading in g m^{-3}) and $Q_1 - Q_R$ diabatic heating (contours in °C h^{-1}) from GPROF Heating algorithm.

Johnson and Hamilton 1988), and those retrieved by the GPROF Heating algorithm (Fig. 4). The LH profile shown in the right-hand panel is also similar to both CRM and observational results.

As Figs. 3, 4, and 5a,b illustrate, regardless of differences in spatial resolution, the instantaneous LH profiles retrieved by the four different algorithms that qualitatively agree with one another for a) tropical cyclones (HH, PRH, and SLH), b) squall lines (GPROF Heating and PRH), and c) tropical oceanic MCSs (PRH and SLH). Quantitatively, there are differences. Some are caused by the different resolutions and filtering techniques employed by the different algorithms, and some by different algorithm inputs. Other differences stem from the varying physical assumptions used by the different algorithms. As one example drawn from the above analyses, PRH consistently produces LH profiles with stronger cooling in the lower troposphere.

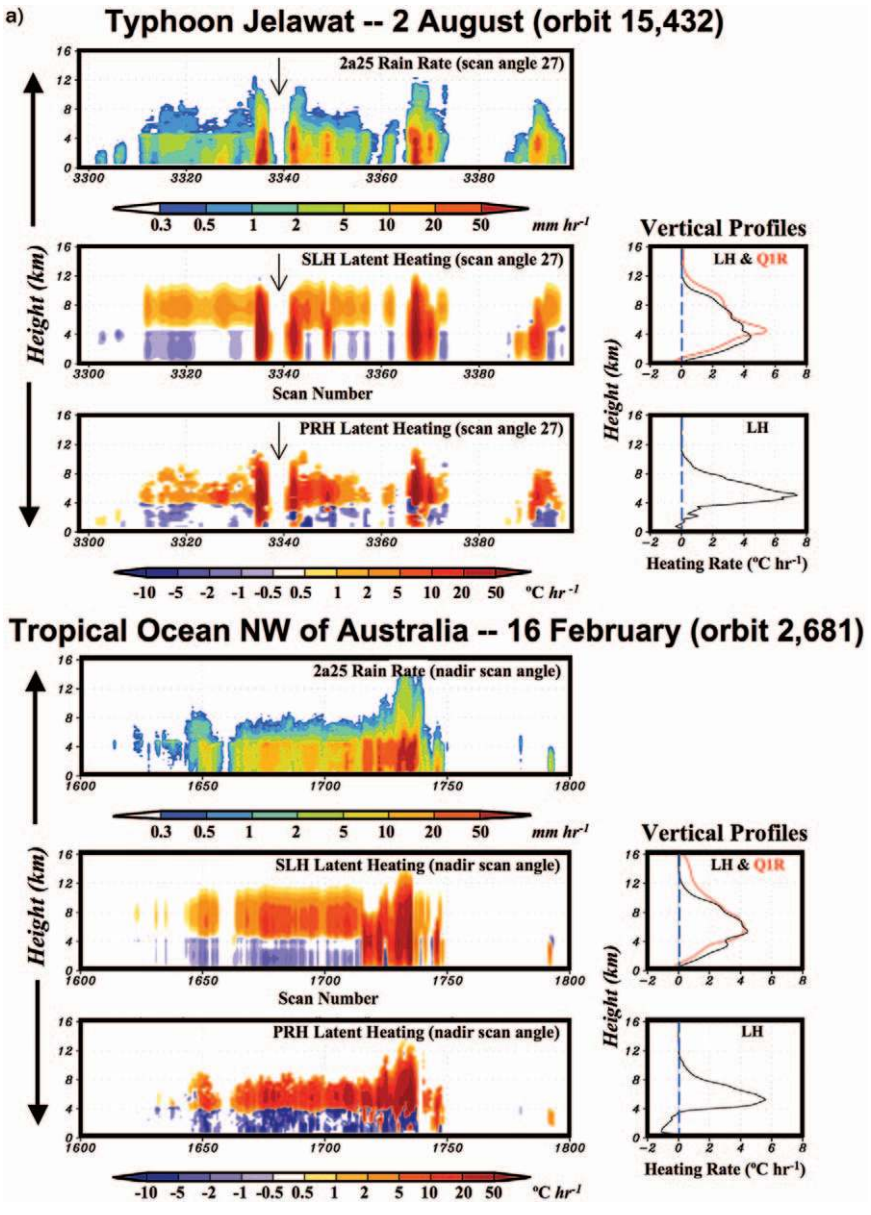

Fig. 5a. (top five) LH analysis for tropical Pacific Typhoon Jelawat in developing stage (2 Aug 2000). Arrows indicate location of eye and (bottom five) identical analysis for tropical, oceanic MCS over northwest Australia (16 Feb 1998). (left) For each set of diagrams height–scan cross sections of PR-based rain-rate profiles (mm h^{-1}), along with SLH- and PRH-generated LH profiles (°C h^{-1}), are shown respectively. [TRMM PR rain-rate algorithm is described by Iguchi et al. (2000) and Meneghini et al. (2000).] (right) area mean vertical profiles of both SLH-generated $Q_1 - Q_R$ (red) and LH (black) and PRH-generated LH (black) in °C h^{-1}, respectively.

Temporal and spatial averages. The upper three panels of Fig. 1 illustrate the 5-yr mean apparent heating at three different altitudes (2, 5, and 8 km) over the global Tropics from the CSH algorithm based upon the PR monthly rainfall product. The Q_1 profiles are calculated by averaging two normalized convective and stratiform kernel heating profiles (scaled according to PR-retrieved surface rain rates and weighted by the convective/stratiform fractions) at a grid scale of 0.5° for either oceanic or continental locations. The normalized convective/stratiform kernel profiles are created by averaging all 16 (4) oceanic (continental) base profiles in the CSH algorithm's complete library of 20 heating profile pairs, which are distributed regionally and according to storm type.

As expected from the design of the CSH algorithm, the horizontal distribution of the estimated Q_1

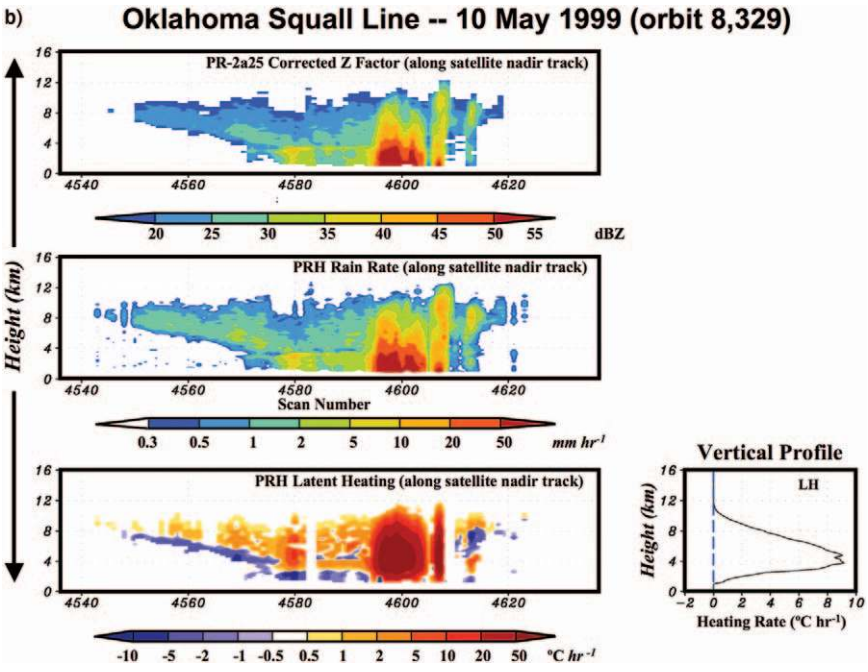

FIG. 5b. Latent heating analysis for midlatitude Oklahoma squall line (10 May 1999). (left) Height–scan cross sections of TRMM PR radar reflectivity profiles (ZE in dBZ), PR-retrieved rain-rate profiles (mm h^{-1}), and PRH-generated LH profiles (°C h^{-1}), all along satellite nadir track. (right) Area mean vertical profile of PRH-generated LH in °C h^{-1}.

structure is similar to the pattern of surface rainfall (lower panel of Fig. 1), especially at the middle and upper levels. For example, well-defined ITCZs in the east and central Pacific and Atlantic Oceans, a well-defined SPCZ in the central southern Pacific Ocean, and broad areas of precipitation events spread over the continental regions are all evident. Also, the strong LH release in the middle and upper troposphere (5°C day^{-1} and greater) is associated with heavier surface precipitation. Heating in the upper troposphere over the Pacific and Indian Oceans covers a much broader area than the heating over Africa, South America, and the Atlantic. The large-scale heating distributions (i.e., differential latent heating) between continents and oceans and within continents and oceans by themselves are capable of altering the ambient horizontal gradients in the temperature fields that then can feed back to the general circulation.

An interesting feature observed in Fig. 1 is the relatively weaker heating at the 2-km level (< 1.5°C day^{-1}), in comparison to the mid- and upper-tropospheric levels, throughout the regions exhibiting the strongest rain rates. Whereas this may be simply convective heating and stratiform cooling in the lower troposphere compensating for one another, it is also possible that this stems from higher moisture contents at lower levels inhibiting evaporative cooling by raindrops in the relatively moister regions.

Figure 6 illustrates the Q_1 structures associated with two climate events: a) an El Niño episode from December 1997 through February 1998, and b) a La Niña episode from December 1998 through February 1999. The diagrams in the two left-hand panels show retrieved heating anomalies for the two events (relative to a 3-yr mean commencing in December 1997). The greatest anomalies appear over the equatorial Pacific, west Pacific, and Indian Oceans. The regional Q_1 anomaly patterns over the Maritime Continent, North America, and Africa are nearly invariant between the two phases. Average Q_1 profiles over the Tropics for these two episodes and their deviations from the 3-yr mean are shown in the right-hand panel. The level of maximum heating is ~7 km. Variations in the level and magnitude of maximum heating are small. This is because global tropical rainfall accumulations for El Niño and La Nina are nearly identical as observed by the PR. However, there are differing cold and warm anomalies associated with the two phases due to the fact that the PR observes a higher percentage of stratiform precipitation during the El Niño episode, leading to the generally stronger low-level cooling.

GLOBAL MODELING APPLICATIONS.

Whereas assimilation of TRMM rainfall data has proven to be an effective technique for improving predictive skill in global weather prediction models (e.g., Bauer et al. 2002; Hou et al. 2000a,b, 2001, 2004; Krishnamurti et al. 2000a,b, 2001; Marecal et al. 2002), the use of explicit LH information for initialization and/or assimilation in global models is a research topic that is just beginning to emerge. Various recent TRMM studies are now reaching beyond the pioneering research in diabatic initialization and assimilation of latent heat information

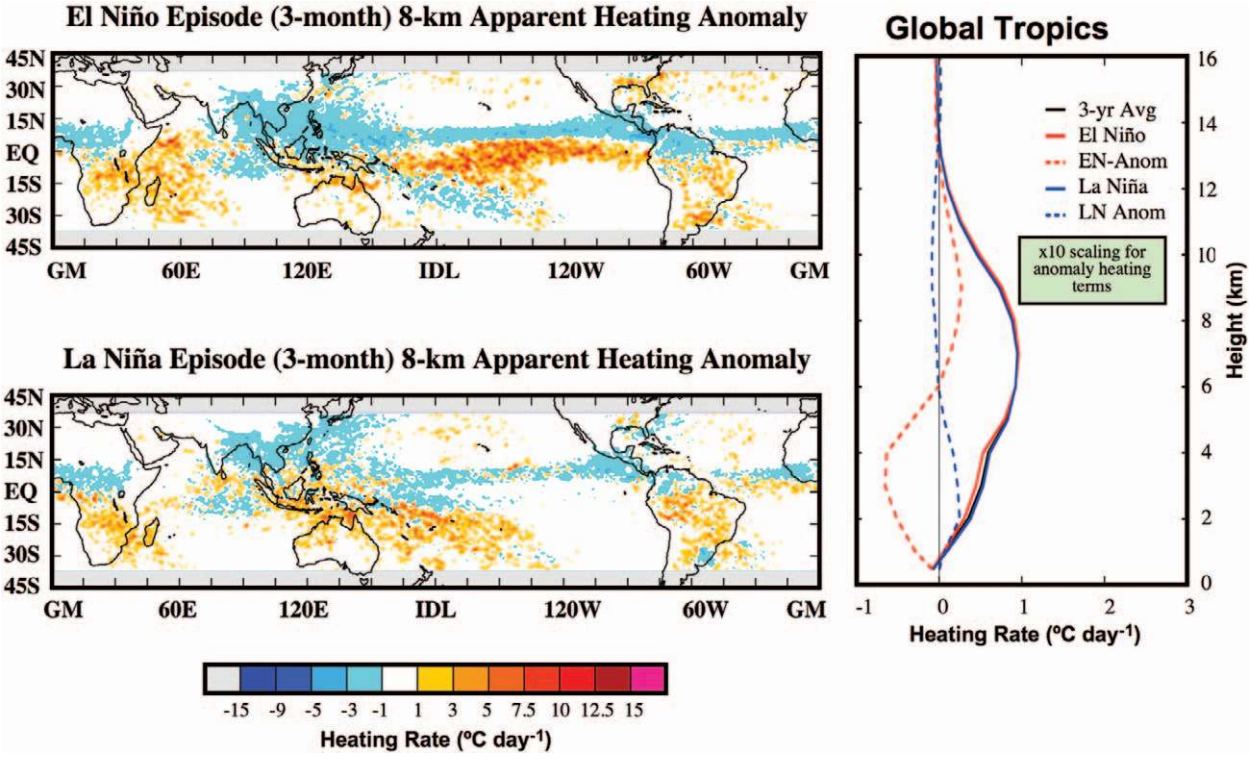

FIG. 6. TRMM PR-based Q_1 heating anomalies at 8 km AGL for (top left) El Niño episode during DJF 1997/98 and (bottom left) La Niña episode during DJF 1998/99 generated from CSH algorithm. (right) Average 3-yr (1997–99), 3-month El Niño episode, and 3-month La Niña episode heating and heating anomaly profile pairs over entire Tropics are shown in black, red, and blue, respectively. [Note: 3-yr profile is indistinguishable from 3-month La Niña profile.]

originally published by Wang and Warner (1988), Puri and Miller (1990), and Raymond et al. (1995). Two global models from The Florida State University (FSU) and the NASA Goddard Space Flight Center (GSFC) are currently using TRMM-based LH datasets to improve cumulus parameterization schemes while at the same time addressing physical shortcomings with the schemes.

At this stage it appears that the direct use of satellite diabatic heating profile information for atmospheric modeling is best accomplished using physical initialization. For example, T. N. Krishnamurti and his colleagues at FSU, using the Krishnamurti et al. (1991) global spectral model as the host, have developed a new experimental cumulus parameterization scheme (ECPS). Past model analysis datasets are used to relate $Q_1 - Q_R$ to TRMM-retrieved LH. Tests are now being conducted with the ECPS in conjunction with a Q_1/Q_2 estimation scheme to produce vertical distributions of heating and moistening for a cumulus environment.

Figure 7 shows test results of ECPS that improve a precipitation forecast over a 72-h period relative to a control run without ECPS. The comparison between the ECPS run (lower panel) and the GPCP satellite observations at verification time (upper panel) are much closer in agreement than is shown by the control forecast (middle panel). The control run produces far too much equatorial rain and generally too little precipitation at the middle latitudes and over tropical Africa in comparison to the ECPS run. Also, the ECPS run produces a more realistic ITCZ (i.e., a system of MCSs and squall lines rather than the widespread rain). This confirms that explicit assimilation of satellite-retrieved LH profiles can produce a positive impact on a forecast. This is significant because it is the vertical distribution of diabatic heating that represents the important forcing on atmospheric circulation, not surface rainfall. However, additional studies will be needed to quantify how much predictive improvement can be obtained on a regular basis in moving from surface rainfall assimilation (and/or PMW Tb assimilation) to LH assimilation.

Research is also taking place at GSFC to develop variational techniques to assimilate TMI-derived convective and stratiform LH rates within the general framework of parameter estimation, using disposable parameters in the relevant moist physics scheme as the control variables. The focus here is to explore

the feasibility of improving global climate analyses and weather forecasts through the assimilation of satellite-retrieved LH profiles that are radiatively compatible with multichannel PMW radiometer radiances. Such optimization of physical parameterizations in the context of data assimilation provides valuable information for diagnosing both model and parameterization deficiencies.

There is a final important application also involving NWP modeling, in which satellite-retrieved LH profiles represent a valuable data resource. As the number of NWP models subjected to initialization by retrieved LH profiles increases, substantitive improvements in forecasts via "superensemble" techniques are expected to take place. The superensemble approach is a powerful tool for improving the robustness of weather and climate forecasts, as has been emphasized in studies from the FSU modeling group (i.e., Krishnamurti et al. 2001). The goal of superensemble forecasting is to reduce overall uncertainties while better estimating errors associated with the various models, their physical parameterizations, and the ingested datasets.

FINAL REMARKS AND RECOMMENDED FUTURE RESEARCH.

Three of the TRMM LH algorithms (i.e., CSH, GPROF Heating, and SLH) use CRM-simulated cloud datasets involving precalculated heating profiles. Given the concern with systematic errors arising from too few available CRM simulations, creating "gaps" in the algorithm-supporting databases, the number of heating profiles associated with different types of clouds and convective systems occurring at a variety of geographic locations and throughout the seasonal cycle needs to be increased. Observations from additional field experiments will also be needed to provide new types of initial conditions for CRMs, as well as validation of the CRM-simulated LH calculations. Heating profiles obtained from numerical model simulations and large-scale model reanalyses should also be compared with those from CRMs and the associated retrieval algorithms.

Such comparisons will identify the key physical processes leading to similarities and differences produced by the CRMs and the retrieval algorithms. Data from field campaigns that provide extensive, high-quality in situ microphysical observations, including TRMM LBA and KWAJEX, will be most useful in validating and improving CRM-generated microphysics. Marzano et al. (1999), Panegrossi et al. (1998), and Fiorino and Smith (2006) have already addressed critical issues concerning how realistic microphysical representations can be used to improve precipitation retrieval algorithms, an essential step in better estimating LH.

It is important that diagnostically based heating profiles obtained from TRMM field campaign

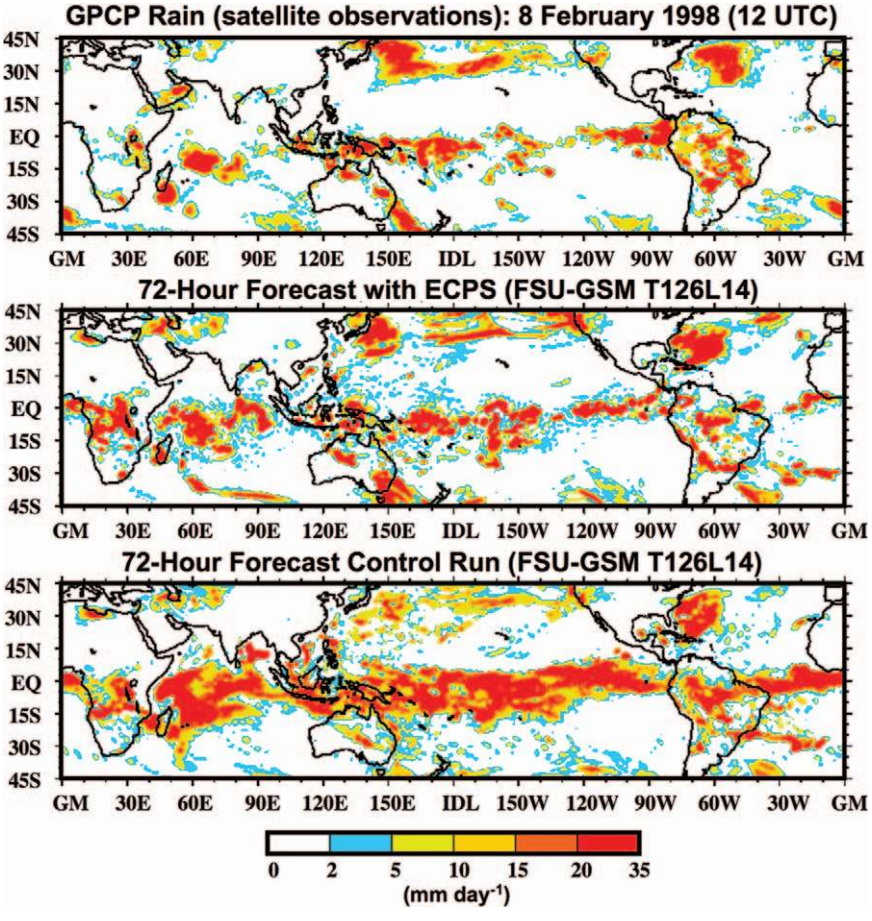

Fig. 7. (top) GPCP precipitation for 8 Feb 1998 representing blend of satellite retrievals and rain gauge observations, (middle) FSU GSM day-2 forecast from ECPS experiment, and (bottom) FSU GSM day-2 forecast from control experiment. [From Rajendran et al. (2004).]

data, as well as from other field campaigns such as those conducted by the DOE ARM program, be compared to corresponding heating profiles from the LH algorithms. This would include diagnostic analyses based on the use of Doppler radar measurements to infer horizontal wind divergence and vertical motion, which are directly related to diabatic heating (e.g., Mapes and Lin 2005), and dual-Doppler measurements that explicitly provide the horizontal wind field [e.g., see the DOE ARM–related paper by Clothiaux et al. (2000)]. These analyses will help quantify errors within the current LH algorithms, plus provide insight for overall algorithm improvements.

As a follow-up to this study, a comprehensive intercomparison between the different LH algorithms applied to various common TRMM datasets has been initiated. This effort will be consistent with past intercomparisons efforts involving precipitation retrieval algorithms (e.g., Ebert and Manton 1998; Smith et al. 1998; Adler et al. 2001) and the radiative transfer models underpinning these algorithms (e.g., Smith et al. 2002). Here the emphasis has been on understanding the strengths and weaknesses of different methods and underlying assumptions, an indispensable process for guiding generational upgrades in algorithm philosophy and design.

The new LH algorithm intercomparison study will focus on the major heat budget terms

$$[\text{i.e., LH, } Q_1, \ Q_R \text{ and } \ \overline{\pi(\partial w'\theta'/\partial z)}].$$

Global analyses will be used to identify and compare the large-scale circulation patterns for important retrieval periods and for key periods of earlier field campaigns, including the GATE and TOGA COARE tropical ocean campaigns. These will be useful because extending what is learned from local field campaign observations to other parts of the Tropics where campaigns have yet to be conducted invites the use of LH "similarity" assumptions. Identification of optimal spatial scales and suitable filtering schemes for the reduction of noise in the instantaneous, high-resolution retrievals are other issues that need attention.

Standard LH products from TRMM will represent a valuable new source of data to the research community, products that a decade ago were considered beyond reach. These data products will enable compelling new investigations into the complexities of storm life cycles, diabatic heating controls and feedbacks related to mesosynoptic circulations, and, most importantly, the influence of diabatic heating on the Earth's general circulation and climate.

ACKNOWLEDGMENTS. The authors extend their appreciation to Professors Robert Houze of the University of Washington, Richard Johnson of Colorado State University, Michio Yanai of the University of California, Los Angeles, and Edward Zipser of the University of Utah, whose willingness over the years to discuss their ideas concerning atmospheric latent heating has had a profound influence on various ideas central to this paper. The authors wish to thank to Dr. Kwo-Sen Kuo of the NASA Goddard Space Flight Center for preparing Fig. 1, and to Mr. Ken'ichi Ito of the Remote Technology Center of Japan for preparing Figs. 5a–b. The authors also thank Dr. G. Huffman and two anonymous reviewers for their constructive comments that were used to improve the paper. This research has been supported by an assortment of TRMM Science Team grants under the auspices of both the National Aeronautics and Space Administration (NASA) and the Japan Aerospace Exploration Agency (JAXA).

REFERENCES

Adler, R. F., and E. B. Rodgers, 1977: Satellite-observed latent heat release in a tropical cyclone. *Mon. Wea. Rev.,* **105,** 956–963.

——, C. Kidd, G. Petty, M. Morissey, and H. M. Goodman, 2001: Intercomparison of global precipitation products: The Third Precipitation Intercomparison Project (PIP-3). *Bull. Amer. Meteor. Soc.,* **82,** 1377–1396.

Bauer, P., J.-F. Mahfouf, W. S. Olson, F. S. Marzano, S. DiMichele, A. Tassa, and A. Mugnai, 2002: Error analysis of TMI rainfall estimates over ocean for variational data assimilation. *Quart. J. Roy. Meteor. Soc.,* **128,** 2129–2144.

Biggerstaff, M. I., and R. A. Houze Jr., 1991: Kinematic and precipitation structure of the 10-11 June 1985 squall line. *Mon. Wea. Rev.,* **119,** 3034–3065.

Clothiaux, E. E., T. P. Ackerman, G. G. Mace, K. P. Moran, R. T. Marchand, M. A. Miller, and B. E. Martner, 2000: Objective determination of cloud heights and radar reflectivities using a combination of active remote sensors at the ARM CART sites. *J. Appl. Meteor.,* **39,** 645–665.

Cunning, J. B., 1986: The Oklahoma-Kansas Preliminary Regional Experiment for STORM-Central. *Bull. Amer. Meteor. Soc.,* **67,** 1478–1486.

Dudhia, J., 1993: A nonhydrostatic version of the Penn State–NCAR Mesoscale Model: Validation tests and simulation of an Atlantic cyclone and cold front. *Mon. Wea. Rev.,* **121,** 1493–1513.

Ebert, E. E., and M. J. Manton, 1998: Performance of satellite rainfall estimation algorithms during TOGA COARE. *J. Atmos. Sci.,* **55,** 1537–1557.

Emanuel, K. E., J. D. Neelin, and C. S. Bretherton, 1994: On large-scale circulations in convecting atmospheres. *Quart. J. Roy. Meteor. Soc.,* **120,** 111–1143.

Fiorino, S. T., and E. A. Smith, 2006: Critical assessment of microphysical assumptions within TRMM radiometer rain profile algorithm using satellite, aircraft, and surface datasets from KWAJEX. *J. Appl. Meteor. Climatol.,* **45,** 754–786.

Frank, W. M., and J. L. McBride, 1989: The vertical distribution of heating in AMEX and GATE cloud clusters. *J. Atmos. Sci.,* **46,** 3464–3478.

GATE International Scientific and Management Group, 1974: GATE final international scientific plans. *Bull. Amer. Meteor. Soc.,* **55,** 711–744.

Hack, J. J., and W. H. Schubert, 1990: Some dynamical properties of idealized thermally-forced meridional circulations in the tropics. *Meteor. Atmos. Phys.,* **44,** 101–118.

Haddad, Z. S., E. A. Smith, C. D. Kummerow, T. Iguchi, M. R. Farrar, S. L. Durden, M. Alves, and W. S. Olson, 1997: The TRMM (Day-1) radar/radiometer combined rain-profiling algorithm. *J. Meteor. Soc. Japan,* **75,** 799–809.

Halverson, J. B., T. Rickenbach, B. Roy, H. Pierce, and E. Williams, 2002: Environmental characteristics of convective systems during TRMM-LBA. *Mon. Wea. Rev.,* **130,** 1493–1509.

Hartmann, D. L., H. H. Hendon, and R. A. Houze Jr., 1984: Some implications of mesoscale circulations in tropical cloud clusters for large-scale dynamics and climate. *J. Atmos. Sci.,* **41,** 113–121.

Hou, A. Y., S.-Q. Zhang, A. M. da Silva, and W. S. Olson, 2000a: Improving assimilated global data sets using TMI rainfall and columnar moisture observations. *J. Climate,* **13,** 4180–4195.

——, D. V. Ledvina, A. M. da Silva, S.-Q. Zhang, J. Joiner, R. M. Atlas, G. J. Huffman, and C. D. Kummerow, 2000b: Assimilation of SSM/I-derived surface rainfall and total precipitable water for improving the GEOS analysis for climate studies. *Mon. Wea. Rev.,* **128,** 509–537.

——, S.-Q. Zhang, A. M. da Silva, W. S. Olson, C. D. Kummerow, and J. Simpson, 2001: Improving global analysis and short-range forecasts using rainfall and moisture observations derived from TRMM and SSM/I passive microwave sensors. *Bull. Amer. Meteor. Soc.,* **82,** 659–679.

——, ——, and O. Reale, 2004: Variational continuous assimilation of TMI and SSM/I rain rates: Impact on *GEOS-3* hurricane analyses and forecasts. *Mon. Wea. Rev.,* **132,** 2094–2109.

Houze, R. A., Jr., 1982: Cloud clusters and large-scale vertical motions in the tropics. *J. Meteor. Soc. Japan,* **60,** 396–409.

——, 1989: Observed structure of mesoscale convective systems and implications for large-scale heating. *Quart. J. Roy. Meteor. Soc.,* **115,** 425–461.

——, 1997: Stratiform precipitation in regions of convection: A meteorological paradox. *Bull. Amer. Meteor. Soc.,* **78,** 2179–2196.

——, and A. K. Betts, 1981: Convection in GATE. *Rev. Geophys.,* **19,** 541–576.

Iguchi, T., T. Kozu, R. Meneghini, J. Awaka, and K. Okamoto, 2000: Rain-profiling algorithm for the TRMM precipitation radar. *J. Appl. Meteor.,* **39,** 2038–2052.

Johnson, R. H., 1984: Partitioning tropical heat and moisture budgets into cumulus and mesoscale components: Implication for cumulus parameterization. *Mon. Wea. Rev.,* **112,** 1656–1665.

——, and P. J. Hamilton, 1988: The relationship of surface pressure features to the precipitation and airflow structure of an intense midlatitude squall line. *Mon. Wea. Rev.,* **116,** 1444–1472.

Jorgsensen, D. P., M. A. LeMone, and S. B. Trier, 1997: Structure and evolution of the 22 February 1993 TOGA COARE squall line: Aircraft observations of precipitation, circulation, and surface energy fluxes. *J. Atmos. Sci.,* **54,** 1961–1985.

Krishnamurti, T. N., J. S. Xue, H. S. Bedi, K. Ingles, and D. Oosterhof, 1991: Physical initialization for numerical weather prediction over the tropics. *Tellus,* **43,** 53–81.

——, C. M. Kishtawal, Z. Zhang, T. LaRow, D. Bachiochi, E. Williford, S. Gadgil, and S. Surendran, 2000a: Multimodel ensemble forecasts for weather and seasonal climate. *J. Climate,* **13,** 4196–4216.

——, ——, D. W. Shin, and C. E. Willford, 2000b: Improving tropical precipitation forecasts from a multianalysis supersensemble. *J. Climate,* **13,** 4217–4227.

——, and Coauthors, 2001: Real-time multianalysis-multimodel superensemble forecasts of precipitation using TRMM and SSM/I products. *Mon. Wea. Rev.,* **129,** 2861–2883.

Krueger, S. K., 1988: Numerical simulation of tropical cumulus clouds and their interaction with the subcloud layer. *J. Atmos. Sci.,* **45,** 2221–2250.

Kummerow, C., W. S. Olson, and L. Giglio, 1996: A simplified scheme for obtaining precipitation and vertical hydrometeor profiles from passive microwave sensors. *IEEE Trans. Geosci. Remote Sens.,* **34,** 1213–1232.

——, and Coauthors, 2001: The evolution of the Goddard Profiling Algorithm (GPROF) for rainfall estimation from passive microwave sensors. *J. Appl. Meteor.,* **40,** 1801–1820.

Lang, S., W.-K. Tao., J. Simpson, and B. Ferrier, 2003: Numerical modeling of convective–stratiform pre-

cipitation processes: Sensitivity to partition methods. *J. Appl. Meteor.,* **42,** 505–527.

Lau, K.-M., and L. Peng, 1987: Origin of low-frequency (intraseasonal) oscillations in the tropical atmosphere. Part I: Basic theory. *J. Atmos. Sci.,* **44,** 950–972.

——, and P. H. Chan, 1988: Intraseasonal and interannual variations of tropical convection: A possible link between the 40-day mode and ENSO. *J. Atmos. Sci.,* **45,** 950–972.

——, and Coauthors, 2000: A report of the field operations and early results of the South China Sea Monsoon Experiment (SCSMEX). *Bull. Amer. Meteor. Soc.,* **81,** 1261–1270.

Lipps, F. B., and R. S. Hemler, 1986: Numerical simulation of deep tropical convection associated with large-scale convergence. *J. Atmos. Sci.,* **43,** 1796–1816.

Mapes, B. E., and J. Lin, 2005: Doppler radar observations of mesoscale wind divergence in regions of tropical convection. *Mon. Wea. Rev.,* **133,** 1808–1824.

Marecal, V., J.-F. Mafouf, and P. Bauer, 2002: Comparison of TMI rainfall estimates and their impact on 4D-Var assimilation. *Quart. J. Roy. Meteor. Soc.,* **128,** 2737–2758.

Marzano, F. S., A. Mugnai, G. Panegrossi, N. Pierdicca, E. A. Smith, and J. Turk, 1999: Bayesian estimation of precipitating cloud parameters from combined measurements of spaceborne microwave radiometer and radar. *IEEE Trans. Geosci. Remote Sens.,* **37,** 596–613.

Meneghini, R., T. Iguchi, T. Kozu, L. Liao, K. Okamoto, J. Jones, and J. Kwiatowski, 2000: Use of the surface reference technique for path attenuation estimates from the TRMM Precipitation Radar. *J. Appl. Meteor.,* **39,** 2053–2070.

Nakazawa, T., 1988: Tropical superclusters within intraseasonal variations over the western Pacific. *J. Meteor. Soc. Japan,* **66,** 823–839.

——, 1995: Intraseasonal oscillations during the TOGA-COARE IOP. *J. Meteor. Soc. Japan,* **73,** 305–319.

Nigam, S., C. Chung, and E. DeWeaver, 2000: ENSO diabatic heating on ECMWF and NCEP–NCAR reanalyses and NCAR CCM3 simulation. *J. Climate,* **13,** 3152–3171.

Nitta, T., 1977: Response of cumulus updraft and downdraft to GATE A/B-scale motion systems. *J. Atmos. Sci.,* **34,** 1163–1186.

Olson, W. S., C. D. Kummerow, Y. Hong, and W.-K. Tao, 1999: Atmospheric latent heating distributions in the Tropics derived from passive microwave radiometer measurements. *J. Appl. Meteor.,* **38,** 633–664.

——, and Coauthors, 2006: Precipitation and latent heating distributions from satellite passive microwave radiometry. Part I: Method and uncertainties. *J. Appl. Meteor. Climatol.,* **45,** 702–720.

Panegrossi, G., and Coauthors, 1998: Use of cloud model microphysics for passive microwave-based precipitation retrieval: Significance of consistency between model and measurement manifolds. *J. Atmos. Sci.,* **55,** 1644–1673.

Petersen, W. A., S. W. Nesbitt, R. J. Blakeslee, R. Cifelli, P. Hein, and S. A. Rutledge, 2002: TRMM observations of intraseasonal variability in convective regimes over the Amazon. *J. Climate,* **15,** 1278–1294.

Puri, K., 1987: Some experiments on the use of tropical diabatic heating information for initial state specification. *Mon. Wea. Rev.,* **115,** 1394–1406.

——, and M. J. Miller, 1990: The use of satellite data in the specification of convective heating for diabatic initialization and moisture adjustment in numerical weather prediction models. *Mon. Wea. Rev.,* **118,** 67–93.

Rajendran, T., T. N. Krishnamurti, V. Misra, and W.-K. Tao, 2004: An empirical cumulus parameterization scheme for a global spectral model. *J. Meteor. Soc. Japan,* **82,** 989–1006..

Raymond, W. H., W. S. Olson, and G. Callan, 1995: Diabatic forcing and initialization with assimilated cloud water and rainwater in a forecast model. *Mon. Wea. Rev.,* **123,** 366–382.

Riehl, H., and J. S. Malkus, 1958: On the heat balance in the equatorial trough zone. *Geophysica,* **6,** 503–538.

Rutledge, S. A., R. A. Houze Jr., M. I. Biggerstaff, and T. Matejka, 1988: The Oklahoma–Kansas mesoscale convective system of 10–11 June 1985: Precipitation structure and single-Doppler radar analysis. *Mon. Wea. Rev.,* **116,** 1409–1430.

Satoh, S., and A. Noda, 2001: Retrieval of latent heating profiles from TRMM radar data. *Proc. of the 30th Int. Conf. on Radar Meteorology,* Munich, Germany, Amer. Meteor. Soc., 340–342.

Schumacher, C., R. A. Houze Jr., and I. Kraucunas, 2004: The tropical dynamical response to latent heating estimates derived from the TRMM precipitation radar. *J. Atmos. Sci.,* **61,** 1341–1358.

Shige, S., Y. N. Takayabu, W.-K. Tao, and D. E. Johnson, 2004: Spectral retrieval of latent heating profiles from TRMM PR data. Part I: Development of a model-based algorithm. *J. Appl. Meteor.,* **43,** 1095–1113.

Simpson, J., and W.-K. Tao, 1993: The Goddard Cumulus Ensemble Model. Part II: Applications for studying cloud precipitating processes and for NASA TRMM. *Terr. Atmos. Oceanic Sci.,* **4,** 73–116.

——, C. Kummerow, W.-K. Tao, and R. Adler, 1996: On the Tropical Rainfall Measuring Mission (TRMM). *Meteor. Atmos. Phys.,* **60,** 19–36.

Smith, E. A., X. Xiang, A. Mugnai, and G. Tripoli, 1992: A cloud radiation model for spaceborne precipitation

retrieval. *Extended Abstracts, Int. TRMM Workshop on the Processing and Utilization of the Rainfall Data Measured from Space,* Tokyo, Japan, Communications Research Laboratory, 273–283.

——, ——, ——, and ——, 1994a: Design of an inversion-based precipitation profile retrieval algorithm using an explicit cloud model for initial guess microphysics. *Meteor. Atmos. Phys.,* **54,** 53–78.

——, A. Mugnai, and G. Tripoli, 1994b: Theoretical foundations and verification of a multispectral, inversion-type microwave precipitation profile retrieval algorithm. *Passive Microwave Remote Sensing of Land–Atmosphere Interactions,* VSP Press, 599–621.

——, J. Turk, M. Farrar, A. Mugnai, and X. Xiang, 1997: Estimating 13.8-GHz path integrated attenuation from 10.7-GHz brightness temperatures for TRMM combined PR-TMI precipitation algorithm. *J. Appl. Meteor.,* **36,** 365–388.

——, and Coauthors, 1998: Results of WetNet PIP-2 project. *J. Atmos. Sci.,* **55,** 1483–1536.

——, P. Bauer, F. S. Marzano, C. D. Kummerow, D. McKague, A. Mugnai, and G. Panegrossi, 2002: Intercomparison of microwave radiative transfer models in precipitating clouds. *IEEE Trans. Geosci. Remote Sens.,* **40,** 541–549.

——, and Coauthors, 2006: International Global Precipitation Measurement (GPM) program and mission: An overview. *Measuring Precipitation from Space: EURAINSAT and the Future,* V. Levizzani, P. Bauer and F. J. Turk, Eds., Springer Verlag, in press.

Soong, S.-T., and W.-K. Tao, 1980: Response of deep tropical clouds to mesoscale processes. *J. Atmos. Sci.,* **37,** 2016–2036.

——, and Coauthors, 1984: A numerical study of the vertical transport of momentum in a tropical rainband. *J. Atmos. Sci.,* **41,** 1049–1061.

Stokes, G. M., and S. E. Schwartz, 1994: The Atmospheric Radiation Measurement (ARM) Program: Programmatic background and design of the Cloud and Radiation Test Bed. *Bull. Amer. Meteor. Soc.,* **75,** 1201–1222.

Sui, C.-H., and K.-M. Lau, 1988: Origin of low-frequency (intraseasonal) oscillations in the tropical atmosphere. Part II: Structure and propagation of mobile wave-CISK modes and their modification by lower boundary forcings. *J. Atmos. Sci.,* **46,** 37–56.

Sumi, A., and T. Nakazawa, 2002: Satellite monitoring for the season-to-interannual climate fluctuations. *Korean J. Atmos. Sci,* **5S,** 13–28.

Takayabu, Y. N., 2002: Spectral representation of rain features and diurnal variations observed with TRMM PR over the equatorial areas. *Geophys. Res. Lett.,* **29,** 1584, doi:10.1029/2001GL014113.

Tao, W.-K., 2003: Goddard Cumulus Ensemble (GCE) Model: Application for understanding precipitation processes. *Cloud Systems, Hurricanes, and the Tropical Rainfall Measuring Mission (TRMM): A Tribute to Dr. Joanne Simpson, Meteor. Monogr.,* No. 29, Amer. Meteor. Soc., 107–138.

——, and S.-T. Soong, 1986: A study of the response of deep tropical clouds to mesoscale processes: Three-dimensional numerical experiments. *J. Atmos. Sci.,* **43,** 2653–2676.

——, and S.-T. Soong, 1987: Statistical properties of a cloud ensemble: A numerical study. *J. Atmos. Sci.,* **44,** 3175–3187.

——, and J. Simpson, 1993: The Goddard Cumulus Ensemble Model. Part I: Model description. *Terr. Atmos. Oceanic Sci.,* **4,** 19–54.

——, ——, S. Lang, M. McCumber, R. Adler, and R. Penc, 1990: An algorithm to estimate the heating budget from vertical hydrometeor profiles. *J. Appl. Meteor.,* **29,** 1232–1244.

——, C.-H. Sui, B. Ferrier, S. Lang, J. Scala, M.-D. Chou, and K. Pickering, 1993a: Heating, moisture and water budgets of tropical and mid-latitude squall lines: Comparisons and sensitivity to longwave radiation. *J. Atmos. Sci.,* **50,** 673–690.

——, S. Lang, J. Simpson, and R. Adler, 1993b: Retrieval algorithms for estimating the vertical profiles of latent heat release: Their applications for TRMM. *J. Meteor. Soc. Japan,* **71,** 685–700.

——, J. Scala, B. Ferrier, and J. Simpson, 1995: The effects of melting processes on the development of a tropical and a mid-latitudes squall line. *J. Atmos. Sci.,* **52,** 1934–1948.

——, J. Simpson, S. Lang, C.-H. Sui, B. Ferrier, and M.-D. Chou, 1996: Mechanisms of cloud-radiation interaction in the Tropics and mid-latitudes. *J. Atmos. Sci.,* **53,** 2624–2651.

——, S. Lang, J. Simpson, W. S. Olson, D. Johnson, B. Ferrier, C. Kummerow, and R. Adler, 2000: Retrieving vertical profiles of latent heat release in TOGA COARE convective systems using a cloud resolving model, SSM/I and radar data. *J. Meteor. Soc. Japan,* **78,** 333–355.

——, and Coauthors, 2001: Retrieved vertical profiles of latent heating release using TRMM rainfall products for February 1998. *J. Appl. Meteor.,* **40,** 957–982.

——, and Coauthors, 2003: Microphysics, radiation and surface processes in the Goddard Cumulus Ensemble (GEC) model. *Meteor. Atmos. Phys.,* **82,** 97–137.

Tripoli, G. J., 1992a: A nonhydrostatic mesoscale model designed to simulate scale interaction. *Mon. Wea. Rev.,* **120,** 1342–1359.

——, 1992b: An explicit three-dimensional nonhydrostatic simulation of a tropical cyclone. *Meteor. Atmos. Phys.,* **49,** 229–254.

——, and W. R. Cotton, 1989a: Numerical study of an observed orogenic mesoscale convective system: 1. Simulated genesis and comparison with observations. *Mon. Wea. Rev.,* **117,** 273–304.

——, and ——, 1989b: Numerical study of an observed orogenic mesoscale convective system: 2. Analysis of governing dynamics. *Mon. Wea. Rev.,* **117,** 305–328.

Wang, W., and T. T. Warner, 1988: Use of four-dimensional data assimilation by Newtonian relaxation and latent-heat forcing to improve a mesoscale-model precipitation forecast: A case study. *Mon. Wea. Rev.,* **116,** 2593–2613.

Wang, Y., W.-K. Tao, and J. Simpson, 1996: The impact of ocean surface fluxes on a TOGA COARE convective system. *Mon. Wea. Rev.,* **124,** 2753–2763.

Webster, P. J., and R. Lukas, 1992: TOGA COARE: The coupled ocean–atmosphere response experiment. *Bull. Amer. Meteor. Soc.,* **73,** 1377–1416.

Yanai, M., S. Esbensen, and J. Chu, 1973: Determination of average bulk properties of tropical cloud clusters from large-scale heat and moisture budgets. *J. Atmos. Sci.,* **30,** 611–627.

——, B. Chen, and W.-W. Tung, 2000: The Madden–Julian oscillation observed during the TOGA COARE IOP: Global view. *J. Atmos. Sci.,* **57,** 2374–2396.

Yang, S., and E. A. Smith, 1999a: Moisture budget analysis of TOGA COARE area using SSM/I-retrieved latent heating and large-scale Q_2 estimates. *J. Atmos. Oceanic Technol.,* **16,** 633–655.

——, and ——, 1999b: Four-dimensional structure of monthly latent heating derived from SSM/I satellite measurements. *J. Climate,* **12,** 1016–1037.

——, and ——, 2000: Vertical structure and transient behavior of convective–stratiform heating in TOGA-COARE from combined satellite-sounding analysis. *J. Appl. Meteor.,* **39,** 1491–1513.

——, W. S. Olson, J.-J. Wang, T. L. Bell, E. A. Smith, and C. D. Kummerow, 2006: Precipitation and latent heating distributions from satellite passive microwave radiometry. Part II: Evaluation of estimates using independent data. *J. Appl. Meteor. Climatol.,* **45,** 721–739.

Yuter, S. E., R. A. Houze Jr., E. A. Smith, T. T. Wilheit, and E. Zipser, 2005: Physical characterization of tropical oceanic convection observed in KWAJEX. *J. Appl. Meteor.,* **44,** 385–415.